RESEARCH PAPER

PCCP
www.rsc.org/pccp

Measurement of diffusion in Langmuir monolayers by single-particle tracking†

Carsten Selle,*[a] Florian Rückerl,[a] Douglas S. Martin,[b] Martin B. Forstner[b] and Josef A. Käs[a]

[a] *Institute of Experimental Physics I, University of Leipzig, Linnestraße 5, D-04103 Leipzig, Germany. E-mail: selle@physik.uni-leipzig.de; Fax: +49 341 9732479; Tel: +49 341 9732573*
[b] *Center for Nonlinear Dynamics, University of Texas, Austin, TX, USA*

Received 17th August 2004, Accepted 28th October 2004
First published as an Advance Article on the web 15th November 2004

There is a great amount of literature available indicating that membranes are inhomogeneous, complex fluids. For instance, observation of diffusion in cell membranes demonstrated confined motion of membrane constituents and even subdiffusion. In order to circumvent the small dimensions of cells leading to weak statistics when investigating the diffusion properties of single membrane components, a technique based on optical microscopy employing Langmuir monolayers as membrane model systems has been developed in our lab. In earlier work, the motion of labeled single lipids was visualized. These measurements with long observation times, thus far only possible with this method, were combined with respective Monte-Carlo simulations. We could conclude that noise can lead in general to the assumption of subdiffusion while interpreting the results of single-particle-tracking (SPT) experiments within membranes in general. Since the packing density of lipids within monolayers at the air/water interface can be changed easily, inhomogeneity with regard to the phase state can be achieved by isothermal compression to coexistence regions. Surface charged polystyrene latexes were used as model proteins diffusing in inhomogeneous monolayers as biomembrane mimics. Epifluorescence microscopy coupled to SPT revealed that domain associated, dimensionally reduced diffusion can occur in these kinds of model systems. This was caused by an attractive potential generated by condensed domains within monolayers. Monte-Carlo simulations supported this view point. Moreover, long-time simulations show that diffusion coefficients of respective particles were dependent on the strength of the attractive potential present: a behavior reflecting altered dimensionality of diffusion. The widths of those potentials were also found to be affected by the domain size of the more ordered lipid phase. In biological membrane systems, cells could utilize these physical mechanisms to adjust diffusion properties of membrane components.

1. Introduction

Lateral transport plays a key role in biological processes such as, *e.g.* cellular signal transduction within the cell membrane and membrane formation. The transport of a signal mediated by components of a membrane can occur through lateral diffusion.[1] Reactions dependent on diffusion may proceed faster in the two dimensions of the membrane than in the three dimensions of the cytoplasm.[2] The two-dimensional liquid-crystalline membranes generally consist in a diverse amphiphilic lipid bilayer where proteins are differently integrated. Membranes seem to be relatively homogenous systems where lateral diffusion could be described easily. However, it was found that the cell membrane is inhomogeneous over different time and length scales.[3] Inhomogeneity was experimentally shown for the two main classes of membrane components, both for lipids and for proteins, by demonstration of restricted mobility. The motion of proteins can be confined to regions of 100 nm to 1 μm size for a time from 3–35 s. The actual size of these confinements for the lateral protein motion seems to be dependent on the cell type investigated.[4–8] Using optical tweezers, barrier free lengths for proteins of 1–10 μm were found.[9]

Lipid diffusion within a membrane can be confined for times of less than a second to regions of 250–750 nm size within the cell membrane.[10,11] However, free diffusion was observed for lipids within a membrane, too.[12]

Furthermore, the diffusive speed of integral proteins in biological membranes is decreased by one order of magnitude up to immobility compared to the less complex model membranes.[13]

Disturbing interactions of diffusing proteins with other structures within the membrane, *e.g.* with the membrane-associated cytoskeleton or ordered lipid domains, are supposed to be the reasons for this behavior.[7,14,15]

Membrane components coming into question as potential obstructions can be arranged according to their size. Proteins (25–75% of membrane mass[16]) can be considered as a first category of obstacles on a length scale of few nanometers. As a second category, proteins with condensed lipid shells of a 10 nm diameter come into play.[17] Lipid rafts, as a potential third category, presumably have a size of 25–300 nm and represent mobile lipid organizations which differ with respect to their composition from their environment.[10,14,18–21] There are numerous indications that lipid rafts might play also a central role in diseases as, *e.g.* virus infections, Alzheimer and prion diseases.[22] Nevertheless, thus far these ordered domains could not be directly observed. Their occurrence was merely indirectly deducted, *e.g.*, from protein-clustering experiments.[11]

Hence, the biological membrane is currently considered to be an inhomogeneous fluid with structures on length scales of 1 nm to 10 μm which affect the lateral diffusion[15].

Diffusion of a laterally moving particle within the membrane can be described by the temporal scaling behavior of the mean square displacement (MSD) in dependence on the time Δt [23]

$$\langle r^2 \rangle = \mathrm{MSD}(\Delta t) = 4D\Delta t^{\alpha} \qquad (1)$$

† Presented at the annual meeting of the Deutsche Bunsen-Gesellschaft für Physikalische Chemie, Dresden, Germany, May 20–22, 2004.

DOI: 10.1039/b412680g

where $\boldsymbol{r}(t)$ is the particle position at the time t, D the diffusion coefficient and α the scaling exponent. For normal Brownian diffusion, the exponent α remains 1. Subdiffusive processes exhibit $\alpha < 1$. Anomalous, non-Brownian diffusion was reported for different membrane components. For proteins in the plasma membrane, exponents in the range of $\alpha = 0.1$–0.9 were found.[5,24,25] However, evidence for the occurrence of subdiffusion by single-particle-tracking methods is often based on short trajectories where the scaling arguments can be inaccurate.

In order to understand the results on membrane diffusion experiments, computer simulation methods were developed and performed. Molecular dynamics calculations of the interactions of proteins, lipids and water molecules were carried out but the corresponding length scale is limited to very short distances ($\sim$1 nm).[26] The diffusion constants obtained (1–10 $\mu m^2\ s^{-1}$) agree with those from spectroscopic measurements. Monte Carlo methods can give results regarding diffusion on length scales which correspond to those of fluorescence recovery after photobleaching (FRAP) and SPT data (in the range of 10^{-9}–10^{-6} m).[27–30] Results of these simulations show, *e.g.* that a 10- to 100-fold decrease of the diffusion coefficient can arise from protein concentrations close to the percolation threshold. At protein concentration above the percolation threshold, only confined diffusion is found. The former appears at long times normal whereas it may appear at short times as anomalous.[29] The implementation of particle traps made the simulation of anomalous diffusion possible.[31]

Increasing interest in understanding the basis of lipid and protein diffusion led to the development of various experimental models of the cell membrane, *e.g.* lipid vesicles with incorporated proteins,[32] planar supported bilayers,[33] with one or more membrane double layers on solid supports which were used for lipid and protein diffusion measurements.[34,35] Within the scope of earlier studies homogeneous one-component systems were investigated.[36] Later, full membrane extracts[37] or multi-component systems in which phase separated lipids form obstructions for diffusion were studied.[38] Currently, the lipid raft mixtures have been frequently investigated by different methods.[8,39]

Monolayers at the air/water interface have a critical advantage over cells and lipid vesicles regarding the investigation of diffusion by SPT techniques. This is the large observable area leading to long observation times. Moreover, the packing density of a monolayer at the air/water interface can be conveniently varied at a constant temperature which is not possible for supported bilayers. In Langmuir monolayers, a broad variable range of length scales within inhomogeneous structures is accessible. In the phase coexistence region *e.g.* in the liquid-expanded/liquid-condensed coexistence, inhomogeneities are characteristic and the size of occurring domains can be varied by altering the lateral pressure.

In the following section, recent achievements in developing the method of SPT on Langmuir monolayers are briefly summarized.

To verify our experimental approach, at first the diffusion of lipids within homogeneous monolayers was studied. In a second step, the motion of carboxylated polystyrene beads within inhomogeneous monolayers was examined. This system mimics the interaction between negatively charged proteins and condensed membrane domains. Already published features of these experimental models are reported concisely in the following. The methods used for experiments and simulations of the model are described in Section 3. New results on these models and interpretations are presented and discussed in significant extracts in Section 4.

2. Single-particle-tracking on monolayers

In our lab, a technique was established enabling single-particle-tracking (SPT) experiments in monolayers at the air/water-interface. In order to obtain a highly unperturbed monolayer, air flow, convection in the subphase and vibrations of the system had to be minimized. For this purpose, a Langmuir film balance system was designed and built that reduces these effects by isolation of the liquid surface from the lab environment. Tracking of the motion of a scattering gold nano particle bound to a single lipid molecule within a monolayer at the air/water interface over long time intervals by means of dark field microscopy was demonstrated. DMPC monolayers were used which form homogeneous phases under standard conditions.[40] For this system, only normal diffusion can be expected according to the free-volume model for diffusion.[41]

Pictures were recorded by use of an appropriate video microscopy system with a time resolution of 30 s^{-1}. Observation times for the tracking experiments ranged up to about 150 s. The particle position per frame was determined applying modified IDL routines.[42] Due to the specific set-up, drift speed of the monolayer was reduced to <1 $\mu m\ s^{-1}$. Nevertheless, for the calculation of the MSD due to pure diffusive motion the relative motion of two neighboring particles with position $\boldsymbol{a}$ and $\boldsymbol{b}$ was utilized. For calculation of the MSD of the relative motion, the following relation was used[43]

$$\mathrm{MSD}_{\mathrm{rel}}(\Delta t) = \left\langle (\boldsymbol{a}-\boldsymbol{b})^2 \right\rangle = \frac{1}{N-n}\sum_{j=1}^{N-n}((\boldsymbol{a}(j\delta t - n\delta t) - \boldsymbol{b}(j\delta t - n\delta t)) - (\boldsymbol{a}j\delta t - \boldsymbol{b}j\delta t))^2 \quad (2)$$

where $\boldsymbol{r}(t)$ is the position of the particle at time t, δt is the time between frames (successive images), Δt is the time lag separating the locations such that $n\delta t = \Delta t$, with n the number of frames separating the locations, and N is the total number of steps in the trajectory. It was demonstrated that the measured diffusive speed of the lipid was independent on the size of the gold particle. The scaling exponent was obtained by a linear fit of log(MSD) *vs.* log(Δt) (*cf.* eqn. (3), below). For DMPC at the air/water interface and different packing densities normal diffusion was found. The diffusion coefficients were obtained by a linear fit of the data to eqn. (1). The diffusion coefficient $D = (1.1 \pm 0.2)\ \mu m^2\ s^{-1}$ was in good agreement with the results from other measurements obtained by ensemble methods, *e.g.* FRAP.[44] Further details are given in the respective previously published manuscript.[43]

According to eqn. (1), the standard method to find the scaling exponent is a linear fit to:

$$\log(\mathrm{MSD}(\Delta t)) = \alpha \log(\Delta t) + \log(4D) \quad (3)$$

Indications for the occurrence of subdiffusion were apparently found in the experiments with DMPC monolayers. Since subdiffusion can be excluded for such a homogeneous system, an artifact due to basic problems of the data analysis had to be to considered. Correlation with noise inherent to all SPT measurements was initially noted.[43] The position of the particle was determined with a precision of 100 nm. The tracking routine employed finds the center of the particle using a weighted average of pixel intensities, taking the center of this average as the particle position. The position can be shifted by overlapping noise leading to an error in the particle position. Assuming a mean error of the particle position σ, the MSD is dependent on this noise:

$$\mathrm{MSD} = 4D\Delta t + 2\sigma^2 \quad (4)$$

To find the diffusion coefficient for Brownian motion, the linear plot gives D as the slope and $2\sigma^2$ as the intercept. The analysis of the logarithmic plot of the MSD which is used to determine whether a particle behaves subdiffusively is more complex since noise generates an initial slope resulting in an apparent scaling coefficient, α_{app} which might by

expressed by

$$\alpha_{app} = \frac{1}{1 + 2\sigma^2/4D\Delta t} \quad (5)$$

In Fig. 1, a logarithmic plot of Brownian motion with an underlying diffusion coefficient of $D = 1\ \mu m^2\ s^{-1}$ and a varied positional error is displayed. Due to the logarithmic scale, noise appears large at short times whereas at long times the real character of the motion (normal diffusion) becomes obvious. Deviations from the noise-free behavior are significantly visible at short times.

This observation was also supported by Monte Carlo simulations on comparable time scales. Random walks were used to simulate recorded measurements. Particle and noise intensity distributions were assumed to be Gaussian profiles according to experimental findings. The error of the position was determined by comparison of the underlying random walk and the trajectories yielded by the tracking routine. A constant error was obtained which is dependent on the signal-to-noise ratio, the particle width and the tracking method. In the light of these findings, experimental results indicating subdiffusion on cell surfaces have to be re-evaluated. It was concluded that a high fraction of these previously published data[5,6,10] can be explained by the interplay of normal diffusion and camera noise.

In summary, long experimental observation times compared to those possible for SPT studies of the cell surface enabled us to demonstrate that (camera) noise can lead to the assumption of subdiffusion while interpreting the data of single-particle-tracking experiments. More details are available in Martin *et al.*[30]

Direct observation of the effect of membrane inhomogeneities on diffusion of polystyrene beads within the model membranes was achieved by utilization of an experimental setup where dual band fluorescence microscopy was coupled to SPT (for details, *cf.* Forstner *et al.*[45] and Section 3 of this paper). A single trough for spreading the monolayer, compression and observation was used. Two compartments were integrated for surface tension measurement and for observation of the monolayers. This allowed us variation of the lateral pressure during observation. In a first series of experiments, DMPE (1,2-dimyristoyl *sn*-glycerophosphoethanolamine) monolayers[46] were spread on a physiological subphase (phosphate buffered saline, *cf.* Section 3). The liquid expanded (LE) phase was visualized by fluorescently labeled lipids which partitionate preferably into this phase.[47] Fluorescently labeled carboxylated polystyrene latexes mimicking negatively charged proteins (diameter 100 and 200 nm) were added to the subphase and were found to be localized at the air/water interface. The diffusion of the beads within the liquid-expanded (LE) lipid monolayer phase was observed for long time scales. Observation times of up to 20 min were achieved due to the relatively rigid properties of the DMPE liquid-condensed (LC) phase. Free and strikingly confined diffusion to the domain-edge were demonstrated in the LE phase. Domain-edge associated diffusion can be ascribed to an interaction between charged beads and domains. Only normal Brownian diffusion has been found as determined from the scaling exponent which was $\alpha = 0.95 \pm 0.05$ for both free and domain-edge associated diffusion.

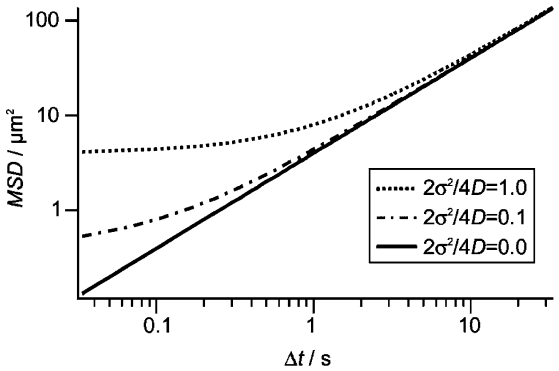

Fig. 1 Typical logarithmic plot of the MSD elucidating how the error in particle position σ can lead to an apparent subdiffusive character of data. The scaling exponent is normally obtained from a logarithmic plot of the MSD(Δt). The constant offset, one possible source might be camera noise, leads to apparent subdiffusion, especially at short times. The diffusion constant D is set to $D = 1\ \mu m^2\ s^{-1}$.

In the following sections, further measurements on bead diffusion in inhomogeneous membranes characterized in another inhomogeneous monolayer system are presented. The strength and the origin of the interaction between beads and domains is analyzed. Simulations were performed to support the interpretation of the experimental findings. Possible consequences for cellular membranes due to the mechanisms found are also discussed.

3. Materials and methods

3.1. Materials

DMPE was purchased from Avanti Polar Lipids (Alabaster, Al, USA), methyl palmitate was from Fluka (Buchs, Switzerland). Salts for the subphase buffer, sodium chloride, monobasic and dibasic sodium phosphate were from Sigma-Aldrich Co. (Steinheim, Germany and St Lois, MO, USA) and of analytical grade. Carboxylated fluorescent microspheres (FluoSpheres, yellow-green fluorescent (505/515), 200 nm diameter, were purchased from Molecular Probes Co. (Leiden, Netherlands)). According to the manufacturer, the surface charge was 0.073 milli-equivalent per gram (data sheet). All chemicals were used without further purification. For filtration of subphase solution, Anotop 25 0.2 μm filters were utilized.

3.2. Sample preparation

The Langmuir trough already mentioned in Section 2[45] was covered by a steel lid with appropriate holes allowing for microscopical observation and measurement of the surface tension. Holes in the lid were sealed against air flow, *e.g.* by a respective ring around the microscope objective and a dome over the Wilhelmy sensor system. Within the trough, smaller observation and surface tension measurement areas were partially separated from the main part of the respective liquid surface by compartments. As a subphase, about 100 ml of potassium-free phosphate buffered saline at pH = 7.5 (PBS, 50 mM NaCl, 50 mM phosphate, ionic strength, I, at 20 °C = 0.189 mol l^{-1}) was prepared using Millipore water.

The diluted aqueous suspension of microspheres was prepared for SPT experiments according to the following procedure. 20 μl of the microsphere suspension as obtained by the manufacturer were diluted in 40 ml of 100 mM PBS buffer, briefly vortexed and then centrifuged at 100 000 *g* for 5 min to ensure the sedimentation of bead conglomerates. 20 ml of the supernatant were transferred into smaller (10 ml) glass bottles. Before each individual experiment, the bead suspension was briefly sonicated (<60 s), to loosen possible weak conglomerates. 35 μl of the diluted suspension were added to the subphase in the Langmuir trough.

Consequentially, monolayers were prepared on the subphase as follows: The lipids (DMPE or methyl palmitate) were dissolved in chloroform (concentration ~0.5 mM) and the resulting solution was then mixed with approx. 0.5–1% (related to DMPE or methyl palmitate concentration) of Texas-Red labeled DPPE (dihexadecanoyl phosphatidylethanolamine) from Molecular Probes (Leiden, Netherlands). This solution was spread on the aqueous surface. The surface drift of the monolayers was reduced to 3–1 μm s^{-1} depending on the phase state of the monolayer allowing for track lengths up to

20 000 to 35 000 steps. All measurements were performed at room temperature ($\vartheta \approx 22$ °C).

3.3. Video microscopy

The lipid monolayer and the fluorescent polysterol latex particles were visualized using an epi-fluorescence microscope (Olympus BX30M, Leeds Instruments Inc, USA) equipped with an Olympus 50 × 0.8 NA darkfield objective, a 100 W Hg-high pressure bulb (Osram HBO 103W/2) and a dual-band filter (51006 FITC/TR Chroma, Brattleboro, VT, USA). Images were recorded by a SIT (Silicon Intensified Tube) Dage-MTI VE 1000 camera (Michigan City, IN, USA,) in PAL or NTSC mode (25 or 30 frames per second, respectively). Data were transfered *via* a frame grabber card (Ni-Daq) connected to a suitable PC system.

3.4. Data analysis

The video files (binary data) were analyzed using a tracking routine in IDL[48] adopted for our system.[43] A Gaussian fit of the pixel intensity was calculated.[49] Other minor modifications of the programs were necessary to change from the NTSC to the PAL system. Up to 50 particles were tracked at once with an estimated spatial accuracy of 100 nm.[30,43] The diffusion coefficients were obtained from a linear fit, the time exponents from logarithmic fits of different data evaluation programs (*cf.* Sections 1 and 2). The length of the tracks was up to 30 min. Immobile fluorescent microspheres within the LC phase (mainly nucleation seeds) were used to determine the collective drift of the surface, which was subtracted from trajectories of diffusing particles. (*cf.* ref. 43, and this paper, Section 2).

3.5. Simulations of random walks

Simulations of random walks can be performed applying pure obstructions in form of LC domains. In this study, random walks were generated with fixed time steps to represent particle trajectories. Following the method described by Saxton,[28] a probability distribution for the step size $\boldsymbol{r}$ was used.

$$P(\boldsymbol{r}) = \frac{1}{4\pi D\delta t}\exp\left[-\frac{\boldsymbol{r}^2}{4D\delta t}\right] \qquad (6)$$

with δt as the time between two steps, which equals 1/25 s due to the camera frame rate used in the experiments. The distribution is inverted to calculate the step size on a uniform random variable [0,1] and the direction is picked randomly from [0,2π].[28] In this fashion, a random walk with a diffusion coefficient D is obtained. In the random walks, generally a diffusion coefficient of 1 $\mu m^2\ s^{-1}$ was applied. The simulation of motion within obstacles is obtained by a simple model for particle domain edge interaction. Particles bounce off the domain edge, the angle of incidence equals the angle of reflection. Thus, when the particle is crossing the domain interface, the particle is reflected, traveling back into the fluid region.

Additionally, the effect an interaction potential was added[50] in order to include interactions between beads and domains.

For a given energy profile $U(\boldsymbol{r})$, the force on the particle $\boldsymbol{F}$, the velocity of the particle $\boldsymbol{v}$, and displacement of the particle $\Delta\boldsymbol{r}$ are calculated from eqns. (7), (8) and (9).

$$\boldsymbol{F}(\boldsymbol{r}) = -\mathrm{d}U(\boldsymbol{r})/\mathrm{d}\boldsymbol{r} \qquad (7)$$

$$\boldsymbol{v} = \boldsymbol{F}/\xi \qquad (8)$$

$$\Delta\boldsymbol{r} = \boldsymbol{v}\delta t \qquad (9)$$

Here, ξ is the friction coefficient of the particle. In each step of the simulation the particle is displaced by $\Delta\boldsymbol{r}$ with regard to the domain boundary.

For a linear relation of $\boldsymbol{F}(\Delta\boldsymbol{r})$, the displacement $\Delta\boldsymbol{r}$ can be calculated from the mean force acting on the particle, *i.e.* from the force at the midpoint of the step. The steptime Δt was chosen such that the actual change in $\boldsymbol{F}$ was not more than 2% from a linear relation. In the neighborhood of the domain where a rapid change of $U(\boldsymbol{r})$ occurs (*cf.* Fig. 2, Sections 4.2 and 4.3) time steps as small as 10^{-9} s were necessary. The random walk was then resampled at the experimental video rate.

For simulating diffusion of particles within a liquid-expanded phase with liquid-expanded domains, a lattice of solid domains was used. The basic tile is a fluid square with a circular solid circle in the center. At an obstacle concentration of 12.5% (circular domains in 4 μm diameter separated by 10 μm) the diffusion of the particles is unchanged from free diffusion. For the latter, the only interaction between probe particle and domain is reflection. This was controlled by evaluation of trajectories with and without obstruction; no difference of diffusion coefficients was found.

4. Results and discussion

4.1. Characteristics of bead diffusion in inhomogeneous membranes

Single-particle tracking experiments were performed with polystyrene beads which are negatively charged due to dissociation of carboxyl groups exposed to the aqueous subphase. This

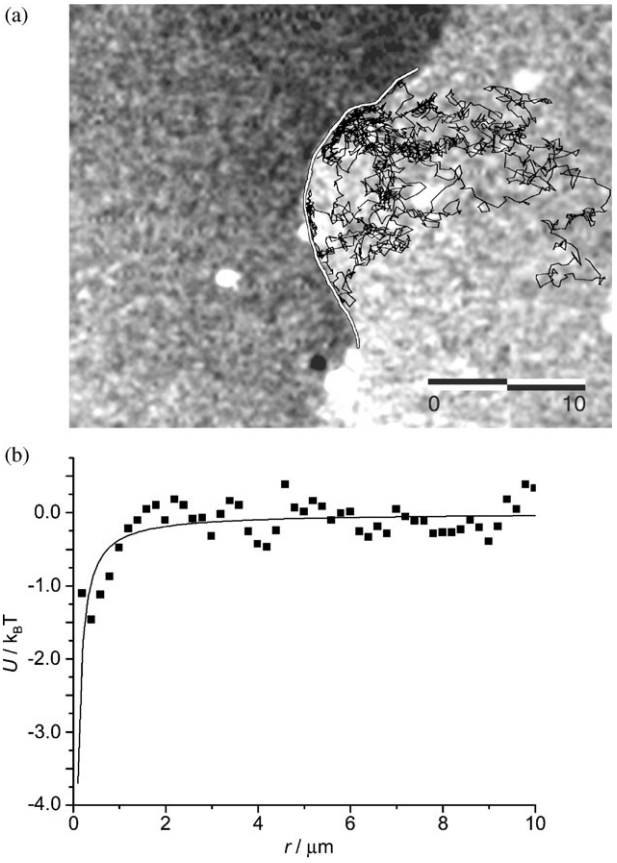

Fig. 2 (a) Epifluorescence microscopic image of carboxylated polystyrene beads within a methyl palmitate monolayer at $\pi = 14$ mN m^{-1} and room temperature. The monolayer displays phase inhomogeneity. The dark area is the LC phase and the bright area is LE phase. Diffusing particles are observed in the LE phase only. The trajectory of 7600 steps is superimposed. Furthermore the domain edge, important for evaluation of the track with regard to the effect of an interaction potential is depicted. The scale bar is 10 μm. (b) From the particle density $\rho(\boldsymbol{r})$, an interaction potential for domains and polystyrene beads can be calculated. The track visualized in (a) leads to an attractive potential of $-4.6k_BT$ depth. For details, see text.

mimics the motion of associated proteins in a membrane. The bead motion within the monolayers was followed by video microscopy as described above. In order to generalize the nature of the model membrane, in a second series of experiments methyl palmitate was applied forming monolayers which are not charged due to the respective molecular structure.

Although two structurally different lipid species, DMPE and methyl palmitate, were studied very similar results were obtained. Thus, the results are presented and discussed together.

Phase coexistence of liquid-expanded and liquid-condensed phases was generated by adjustment of the lateral pressure. This is approximately the case at lateral pressures $\pi > 10$ mN m^{-1} and $\pi > 1$ mN m^{-1} for DMPE and methyl palmitate, respectively. For the polystyrene beads investigated in inhomogeneous monolayers under the experimental conditions, free and domain-edge associated diffusion was observed for both within DMPE[45] and methyl palmitate. The bead motion close to the LC phase is illustrated in Fig. 2A, where the respective superimposed trajectory of a bead diffusing within LE phase and the inhomogeneous monolayer region under observation are shown. This behavior seems to be generally observed for these kinds of model systems. As observed for DMPE[45], within the methyl palmitate monolayers only normal diffusion was found and as can be seen by the value of the scaling exponent $\alpha = 0.99 \pm 0.24$. The results for α derived from individual experimental trajectories for particles within inhomogeneous methyl palmitate monolayers are summarized by the presentation in Fig. 3.

For beads displaying diffusion confined to the domain boundary, reduced diffusion coefficients were found when compared to free diffusion. For free diffusion (no interaction with the domain recognized) diffusion coefficients of 0.75 ± 0.10 μm^2 s^{-1} and 1.31 ± 0.30 μm^2 s^{-1} were obtained for DMPE and methyl palmitate, respectively. For domain-edge associated diffusion the respective values are 0.38 ± 0.05 μm^2 s^{-1}, and 0.41 ± 0.12 μm^2 s^{-1}.

The diffusion coefficient measured for domain-associated bead motion is about one half of the diffusion coefficient of a freely in the monolayer diffusing particle. A transition between two dimensional and one dimensional diffusion explains this since the relations MSD $= 4D\Delta t$ and MSD $= 2D\Delta t$ are valid for two-dimensional and for one-dimensional Brownian diffusion, respectively.

Thus, particles which diffuse only in "one" dimension, *i.e.* along a line (*i.e.* the border of the domain), have a diffusion coefficient only half as large as freely diffusing particles in two dimensions. Further reduction of the coefficient might be explained by additional friction occuring during the movement along the domain border.

4.2. The interaction potential between beads and LC domains

The domain-associated diffusion shown in Fig. 2A for the methyl palmitate model system is apparently due to an attractive interaction between domains and charged beads. A quantitative method to determine an interaction potential $U(\boldsymbol{r})$ is based on the particle density $\rho(\boldsymbol{r})$ as a function of the distance from the domain edge $\boldsymbol{r}$. In other words, $\rho(\boldsymbol{r})$ is the amount of times a specific distance range $[(\boldsymbol{r} - \Delta\boldsymbol{r}), (\boldsymbol{r} + \Delta\boldsymbol{r})]$ from a condensed domain was visited during a track. The size of $\Delta\boldsymbol{r}$ was chosen to values equaling half of the bead diameter. Simulated random walks (*cf.* Section 3) indicated that a higher/lower $\Delta\boldsymbol{r}$ is not feasible. Assuming that the point density follows a Boltzmann distribution[51] one can obtain $U(\boldsymbol{r})$ from $\rho(\boldsymbol{r})$, according to

$$U(\boldsymbol{r}) = -k_B T \log(\rho(\boldsymbol{r})) + C \qquad (10)$$

where the absolute energy can be set by choosing C. In order to calculate $\rho(\boldsymbol{r})$, the amount of times the particle visited area units normalized to equal probabilities of being for the diffusing particle was determined. An example for such an evaluation is given in Fig. 2B which corresponds to the diffusion experiment visualized in Fig. 2A. In this experiment, a polystyrene bead within the LE phase close to a LC phase of a methyl palmitate monolayer clearly demonstrates domain-associated motion. The area close to the interface is obviously more frequently visited during the obversation time. The density $\rho(\boldsymbol{r})$ was calculated and the depth of the attractive potential $U(\boldsymbol{r})$ was obtained setting the constant C so that $U(\boldsymbol{r})$ converges to zero at large distances as depicted in Fig. 2B. The maximal depth at a distance of 100 nm from the domain, corresponding to the polystyrene bead radius, was determined to $U \approx -4.6 k_B T$ by fitting the data using a dependence of $U(\boldsymbol{r}) \sim 1/|\boldsymbol{r}|$. The attractive potentials between LC domains and polystyrene beads obtained by this evaluation method had a depth of $-4.5 \pm 1.0\ k_B T$ and $-6.0 \pm 2.0\ k_B T$ for DMPE and for methyl palmitate monolayers, respectively. The variation of the attractive potentials calculated from our data of bead motion in DMPE monolayers is exemplarily illustrated in Fig. 4. The experimental results of the DMPE system and the evaluation method are discussed in greater detail in a separate contribution.[52]

4.3. Range of the attractive dipole–dipole interactions

In earlier experiments studying the interactions of colloids with lipid domains which were performed employing larger sulfonated polystyrene beads (2.8 μm diameter) and pentadecanoic acid on different subphases, the attractive potentials found could be completely explained by dipolar interactions.[53] We

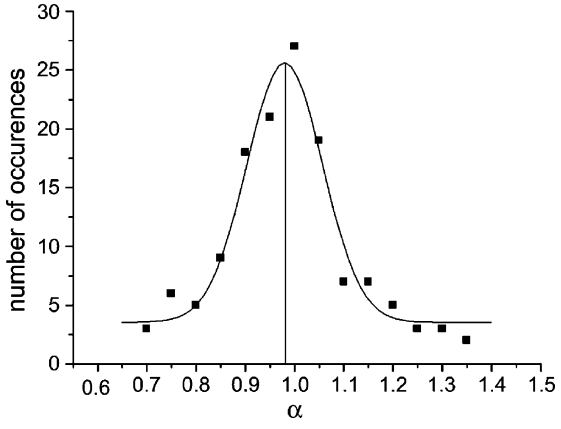

Fig. 3 Distribution of the scaling exponents α found for experiments employing 200 nm carboxylated beads in methyl palmitate. A Gaussian was fitted to the data, yielding a value $\alpha = 0.99 \pm 0.24$.

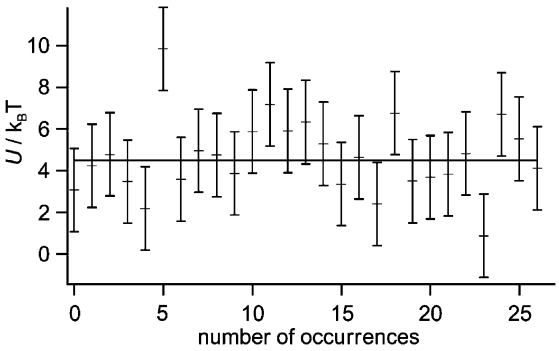

Fig. 4 Potential depths found for attractive interactions between beads and condensed domains. These potentials were calculated from tracks of polystyrene beads within DMPE monolayers in the phase coexistence region. The average potential depth, given for a minimal distance from the domain edge, *i.e.* the bead radius, is represented by a solid line at 4.5 $k_B T$.

also use the approach of these authors in this paper. In the former publication,[53] the diffusion of the particles was not characterized in detail. The focus of interest was on the measurement of the strength of the bead–domain interaction. This strength was reported to be firstly dependent on the electric field generated due dipolar difference within the monolayer between the solid phase and the surrounding fluid, $\Delta\rho_\mu$,[54] and secondly dependent on the dipole moment of the beads, μ_b. The latter can be explained by a charge separation due to a counterion layer in the subphase nearby to the negatively charged sulfonated surface of the polystyrene beads used.[55] We conclude that also the carboxylated beads used in this study have an analogous dipolar moment. It is assumed that the electric field $\boldsymbol{E}$ of the domains in a distance from the domain, $\boldsymbol{r}$, can be calculated from the dipole density difference as follows, where $\boldsymbol{r}_0$ is the radius of the domain and A is the area of the domain:

$$\boldsymbol{E}(\boldsymbol{r}) = \int_A \frac{-\Delta\rho_\mu}{4\pi\varepsilon\varepsilon_0|\boldsymbol{r}-\boldsymbol{r}_0|^3}\,\mathrm{d}\boldsymbol{r}_0 \qquad (11)$$

For the permittivity ε, a value of 7 is used as in ref. 53. This constant accounts for the dielectric properties within the monolayer. The interaction potential with the dipolar moment of a polystyrene bead, μ_b, is calculated as the product of μ_b and $\boldsymbol{E}(\boldsymbol{r})$. The dipolar moment of the bead is $\mu_b = \pi\sigma a^2\lambda_D$ where σ is the charge density on the bead surface, a is the diameter of the bead. λ_D is the Debye length approximated by

$$\lambda_D \approx (0.3)\mathrm{nm}/\sqrt{I} \qquad (12)$$

where I is the ionic strength of the subphase used. As already mentioned above, the potential found, $U(\boldsymbol{r})$ shows a $1/\boldsymbol{r}$ dependence. This behavior is typical if the underlying electric field is generated by a semi-infinite dipolar plate given by:

$$\boldsymbol{E}(\boldsymbol{r}) = \Delta\rho_\mu \frac{2}{4\pi\varepsilon\varepsilon_0}\frac{1}{\boldsymbol{r}} \qquad (13)$$

This situation applies to a small probe particle in front of a large domain. However, the size of domains within inhomogeneous biological membranes is assumed to be 300 nm and less, lying beyond the resolution of optical epifluorescent microscopy used in our experiments. Therefore, the electric field of domains with decreased size, resembling the size of lipid raft microdomains, was calculated by us. For these calculations, an analytical approach published earlier[53] can be used which was derived from eqn. (11). However, this approach is only exact for square domains and distances $\boldsymbol{r} > 2$ μm. In our study, we used two different numerical methods for the calculation of such electric fields which were appropriate for varied domain sizes. One approach we used summarizes over single lipid dipoles located on a hexagonal lattice forming as an entity a circular domain. This method gave consistent results up to domain sizes of 100 nm. The other method is a numerical integration of eqn. (11). The integral is calculated within a 0.5 μm radius of $\boldsymbol{r}$, with a $\mathrm{d}\boldsymbol{r}_0$ that is a square of 10^{-3} μm side length. From 0.5–5 μm, $\mathrm{d}\boldsymbol{r}_0$ is a square of 10^{-2} μm side length. From 5 μm to a cutoff length of 50 μm, $\mathrm{d}\boldsymbol{r}_0$ is a square 0.1 μm side length. This method leads to fields that are accurate to 5% beyond 10^{-2} μm from the edge of a domain and can be used down to domain sizes of 10 nm diameter.[56] For the resulting calculations, the domain radius R was varied from 0.25 nm (~radius of a single lipid chain) to 100 μm. $\boldsymbol{E}(\boldsymbol{r})$ was calculated for 50 nm $< r <$ 20 μm. These calculations indicated a transition in the functional dependence on the distance of the electrical field from a single dipole to the behaviour of an semi-infinite wall. The transition occured at a domain size which is related to the size of potential lipid rafts.

This behavior is illustrated in Fig. 5 which represents the distance dependence of the electric field on R, the domain

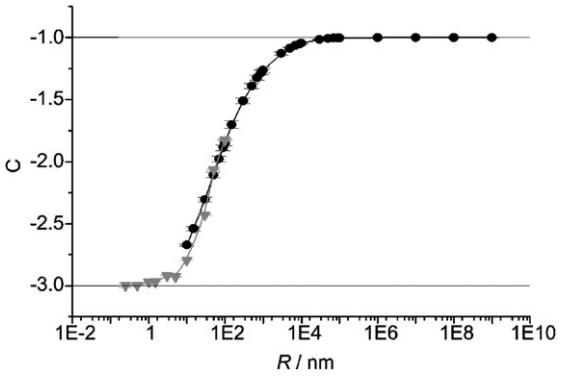

Fig. 5 Due to a difference in dipolar density between the LE phase and the LC phase, *e.g.* in methyl palmitate monolayers, an electric field is formed. The graph depicts the dependence of the scaling parameter C of the proportionality $\boldsymbol{E}(\boldsymbol{r}) \sim 1/\boldsymbol{r}^C$ on the radius R of the respective LC domain. For small domains up to $R = 100$ nm, $\boldsymbol{E}(\boldsymbol{r})$ was calculated by numerical summation over the respective amount of lipid dipoles (triangles). In addition, for $R > 10$ nm, $\boldsymbol{E}(\boldsymbol{r})$ was calculated by numerically integrating over circular domain shapes (circles).

radius. The exponent C for the dependence $\boldsymbol{E} \sim \boldsymbol{r}^C$ was depicted as a function of the exponentially growing domain radius R. For LC domains in a LE phase, a striking increase of C is observed in this representation at a domain size of 10 nm–1000 nm. Therefore, the width of the resulting potential affecting a mobile dipole within the membrane, which is in our experiments a charged latex bead, changes. Some deviation from an ideal curve in the small domain size regime is caused by the use of a hexagonal lattice. These effects of irregularities of the domain border are, as expected, more eminent at small domain sizes.

In short, it can be concluded that the form of the potential and thus its range depend strongly on the size of the domains. In analogy, this suggests for the liquid-ordered/liquid-disordered coexistence in cell membranes with rafts, that the cell might be able to change the range of the domain potentials easily, increasing its ability to influence diffusion processes drastically. This change in size could be achieved by protein clustering processes or by specific fusion of membrane regions with vesicles containing raft lipids. Thus, the cell might control signaling processes and protein reactions by simply growing or shrinking the domains or locally increasing the domain curvature.

4.4. Simulations of dipolar domain–bead interactions

Simulated random walks can be extended far beyond the time scales of the experiments. Furthermore, domain character and

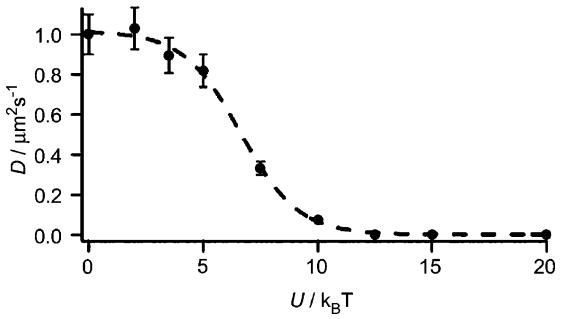

Fig. 6 Long-time diffusion coefficients (in the long-time limit) of particles diffusing in a rectangular lattice with 4 μm diameter domains separated by 10 μm and different attractive interaction potentials. Initial D was set to be 1 $\mu m^2\ s^{-1}$. With increasing potential strengths, particles tend to diffuse localized around the domain boundaries. The diffusion coefficient decreases indicating one-dimensional motion at higher U.

Table 1 Dipolar parameters significant for the systems investigated. Monolayer lipids: DMPE, dimyristoyl phosphatidylethanioamine; MePal, methyl palmitate; PDA, pentadecanoic acid

Systems	$\Delta\rho_\mu/\Delta D$ nm^{-2}	σ/C m^{-2}	μ_b/D	λ_D/nm	U_2/k_BT	U_{th}/k_BT	U_{exp}/k_BT
DMPE[b]	0.05[a]	0.2653	1.749×10^6	0.7	−0.3	−6.1	-4.5 ± 1.0
MePal[b]	0.05–0.2[a]	0.2653	1.749×10^6	0.7	−(0.3–1.2)	−(6.1–24.4)	-6.0 ± 2.0
PDA[c]	0.75[e]	0.0534	2.958×10^8	3.0	−774.4	−1106.2	—[d]
PDA[c]	0.75[e]	0.0534	6.902×10^7	0.7	−180.7	−258.5	—[d]

[a] Values for the dipolar density difference were taken from a reference publication[46] (*cf.* text). [b] Carboxylated polystyrene beads used had a diameter of 200 nm. [c] The parameters were taken from the publication of Nassoy *et al.*,[53] the polystyrene beads had a sulfonated surface and 2.8 μm diameter. U_2 is the dipolar interaction potential calculated for the respective polystyrene bead at a 2 μm distance from the condensed domain edge. U_{th} is the calculated dipolar interaction potential at the minimal distance from the domain edge which equals to half of the respective bead diameter. U_{exp} is the potential depth experimentally found as described in the text. [d] Maximal Potential depths were not explicitly determined. At greater distances $\boldsymbol{r}$, the values found agree well with those calculated. [e] It must be stated however, that Nassoy *et al.* used a wrong value for the dipolar density difference, $\Delta\rho_\mu$, since the given value is the dipolar density calculated from the pure LC phase molecular dipole moment of octadecanoic acid.[57]

potential strength can be altered arbitrarily. In order to study the effect of varied dipolar interaction on diffusion of model proteins within membranes, simulations were carried out assuming varied potential strengths. These simulations were performed under use of 4 μm domains on a 10 μm square lattice. The sole influence of obstacles on the diffusion coefficient under these conditions is negligible (*cf.* methods). The strength of the potential based on dipolar interactions between domain and latex beads applied in these Monte Carlo simulations can be adjusted to fixed values by changing of one of the relevant constants μ_b or $\Delta\rho_\mu$. The trajectories for random walks of 1×10^6 time steps demonstrated high similarity to the experimental results at the relevant potential depths of about 5 k_BT. Domain-associated diffusion was also simulated. From the trajectories, the long-time diffusion coefficient was determined by a linear MSD *vs.* Δt plot. The potential depth (at the minimal distance, $|\boldsymbol{r}| = 50$ nm for 100 nm diameter beads) used was varied in the range from 0 to 20 k_BT. The diffusion coefficient in the long-time limit shows a sharp transition for D from 1 μm^{-2} s^{-1} to about 0 around a potential depth of $U = 6.6k_BT$ (*cf.* Fig. 6). From the graph, it can be concluded that the long-time diffusion constant is apparently very sensitive to the potential in which the particle diffuses.

In the area of the steep decrease in Fig. 6 small variation of the parameters affecting the dipolar interactions in the experiment, *e.g.* by alteration of the packing density of the lipids or change in bead surface charge, should be able to induce significant change in the diffusive behaviour from one-dimensional to two-dimensional and *vice versa*. A change of the potential could be also induced by alteration of the particle nature or the subphase. Small changes in potential can be attributed in various ways to the variability in the bead dipole moment.

For our experiments as well as for the study published by Nassoy *et al.*[53] the relevant dipole interaction parameters of beads and domains are given in Table 1. Moreover, the theoretically achievable maximal attractive potentials are listed and compared to the experimentally observed values. In Nassoy *et al.*'s work, considerably larger beads were chosen leading to dipolar bead moments that were orders of magnitude larger than for the beads we used. However, these authors overestimated the dipolar density difference or excess dipolar density $\Delta\rho_\mu$ since they used a value calculated for the dipolar density of the LC phase of pentadecanoic acid from the molecular dipole moment given for octadecanoic acid in an earlier reference.[57] So, also the calculated potential dependencies as a function of distance from the domain edge must be considered as too high under the conditions assumed by these authors.

For the systems investigated by us, a relatively good agreement can be found comparing the theoretically predicted maximal potentials to the ones obtained experimentally as summarized in Table 1. Here, we rely on the values for $\Delta\rho_\mu$ given by Miller *et al.*[46] For the DMPE system, it is clearly possible to explain the behavior observed by pure dipolar attraction. This approach results in potentials for the DMPE system of $-6.3k_BT$ calculated and $(-4.5 \pm 1.0)k_BT$ measured. For methyl palmitate monolayers, to the best of our knowledge no specific surface potential data are available in the literature. We assume that the $\Delta\rho_\mu$ value for these monolayers is within the range as given for various phospholipids in the cited reference publication.[46] Again, the experimental and theoretically predicted values match relatively well (*cf.* Table 1). The error for the experimentally found potentials might be also considered as too low since the measurements are still away from equilibrium (Boltzmann) conditions. A source for errors in calculating the maximal potential theoretically might be the depth the bead penetrates into the water subphase. This depends strongly on the interaction between the bead surface (carboxyl coated polystyrene) and the aqueous subphase, the surface tension of the monolayer, and the bead–lipid interaction. These factors are not well characterized for the latex beads used for our study. Simple assumptions lead to estimates of the bead penetration of 35%–50% of the total bead diameter.[55] The real penetration depth may be different. Nevertheless, in our case surface interactions seem not to be more significant than for the system used by Nassoy *et al.* The lipid monolayer thickness is about 2 nm, which is very small compared to both the 2.0×10^2 nm and to the 2.8×10^3 nm used in our study studies and by Nassoy *et al.*, respectively. Furthermore, surface charges may vary between different beads and lead to a distribution of interaction strengths. A possible way to address the question if dipolar interaction does explain also the strength of the interaction potential of smaller charged beads within inhomogeneous monolayers would be the use of model proteins that are much smaller by orders of magnitude. The contribution of interface forces to interactions affecting diffusion should be considerably larger for, *e.g.* quantum dots, which have, with their hydrophilic shells, diameters on the order of magnitude of the monolayer thickness.

5. Conclusions

The localization mechanism for diffusing probe particles which can be concluded from our experiments and simulations could enhance reaction kinetics in membranes by increasing the local concentration of reacting components and by restriction of diffusive transport to one dimension. Clustering of proteins, assumed to occur in lipid rafts[21] could be induced by such a mechanism. It is conceivable that the speed of signal transduction is increased drastically by localization of the interacting messengers at the edge of a microdomain. This mechanism is not described yet and could have a similar significance for

reaction kinetics in membranes as the reduction of dimensionality from three to two dimensions which is achieved by integration of proteins into the membranes. A related finding which agrees with our view point was reported in a previous publication describing attractive interaction of concanavalin A protein patches of 1 μm size on water subphases with LC domains within DMPE monolayers.[58] The attractive interaction was explained by different electric polarization of the protein patches and the lipid environment. Penetration of the LC phase boundary by the protein patches was not observed which was explained by packing constraints. The concanavalin A patches have to be considered as macroscopic aggregations and are far away to serve as models for single membrane proteins diffusing in monolayers. Another potential parameter affecting the diffusive behavior was demonstrated to be the size of ordered domains. By the mechanism described in this work, the range of interaction between more ordered domains of potential lipid raft size scale and diffusing charged proteins could be influenced.

Acknowledgements

This research has been funded by the Wolfgang-Paul prize of the Alexander von Humboldt foundation awarded to J. A. K.

References

1 H. Lodish, A. Berk, S. L. Zipurski, P. Matsudaira and D. Baltimore, *Molecular Cell Biology*, W. H. Freeman Co., New York, 2000.
2 G. Adam and M. Delbrück, in *Structural Chemistry and Molecular Biology*, ed. A. Rich and N. Davidson, W. H. Freeman Co., San Francisco, CA, 1968.
3 K. Jacobson, E. D. Sheets and R. Simson, *Science*, 1995, **268**, 144.
4 R. Simson, E. Sheets and K. Jacobson, *Biophys. J.*, 1995, **69**, 989.
5 R. Simson, B. Yang, S. E. Moore, P. Doherty, F. S. Walsh and K. A. Jacobson, *Biophys. J.*, 1998, **74**, 297–308.
6 E. D. Sheets, G. M. Lee, R. Simson and K. Jacobson, *Biochemistry*, 1997, **36**, 12449.
7 A. Kusumi, Y. Sako and M. Yamamoto, *Biophys. J.*, 1993, **65**, 2021.
8 C. Dietrich, B. Yang, T. Fujiwara, A. Kusumi and K. Jacobson, *Biophys. J.*, 2002, **82**, 274.
9 Y. Sako and A. Kusumi, *J. Cell Biol.*, 1995, **129**, 1559.
10 G. J. Schütz, G. Kada, V. P. Pastushenko and H. Schindler, *EMBO J.*, 2000, **19**, 892.
11 T. Fujiwara, K. Ritchie, H. Murakoshi, K. Jacobson and A. Kusumi, *J. Cell Biol.*, 2002, **157**, 1071.
12 M. Vrljic, S. Y. Nishimura, S. Brasselet, W. E. Moerner and H. M. McConnell, *Biophys. J.*, 2002, **83**, 2681.
13 M. Edidin, in *Current Topics in Membranes, Membrane Protein–Cytoskeleton Interactions*, Academic Press, New York, 1996.
14 A. Pralle, P. Keller, E. L. Florin, K. Simons and J. K. Horber, *J. Cell Biol.*, 2000, **148**, 997.
15 G. Vereb, J. Szollosi, J. Matko, P. Nagy, T. Farkas, L. Vigh, L. Matyus, T. A. Waldmann and S. Damjanovich, *Proc. Natl. Acad. Sci. USA*, 2003, **100**, 8053.
16 K. A. Fisher and W. Stoeckenius, *Biomembrane Models in Biophysics*, ed. W. Hoppe, *et al.*, Springer-Verlag, Berlin, 1983.
17 R. G. W. Anderson and K. Jacobson, *Science*, 2002, **296**, 1821.
18 K. Simons and G. Ikonen, *Nature*, 1997, **387**, 569.
19 M. Edidin, *Ann. Rev. Biophys. Biomol. Struct.*, 2003, **32**, 257.
20 E. London and D. A. Brown, *Biochim. Biophys. Acta*, 2000, **1508**, 182.
21 K. Simons and D. Toomre, *Nature (London), Rev. Mol. Cell Biol.*, 2000, **1**, 31.
22 K. Simons and R. Ehehalt, *J. Clin. Invest.*, 2002, **110**, 597.
23 M. J. Saxton and K. Jacobson, *Ann. Rev. Biophys. Biomol. Struct.*, 1997, **26**, 373.
24 T. J. Feder, I. Brust-Mascher, J. P. Slattery, B. Baird and W. W. Webb, *Biophys. J.*, 1996, **70**, 2767.
25 P. R. Smith, I. E. Morrison, K. M. Wilson, N. Fernandez and R. J. Cherry, *Biophys. J.*, 1999, **76**, 3331.
26 R. W. Pastor, R. M. Venable and S. E. Feller, *Acc. Chem. Res.*, 2002, **35**, 438.
27 M. J. Saxton, *Biophys. J.*, 1989, **56**, 615.
28 M. J. Saxton, *Biophys. J.*, 1993, **64**, 1766.
29 M. J. Saxton, *Biophys. J.*, 1994, **66**, 394.
30 D. S. Martin, M. Forstner and J. A. Käs, *Biophys. J.*, 2002, **83**, 2109.
31 M. J. Saxton, *Biophys. J.*, 1996, **70**, 1250.
32 R. Fato, M. Battino, G. Parenti. Castelli and G. Lenaz, *FEBS Lett.*, 1985, **179**, 238.
33 L. K. Tamm and H. M. McConnell, *Biophys. J.*, 1985, **47** 105.
34 G. M. Lee, A. Ishihara and K. A. Jacobson, *Proc. Natl. Acad. Sci. USA*, 1991, **88**, 6274.
35 M. Fein, J. Unkeless, F. Y. S. Chuang, M. Sassroli, R. Dacosta, H. Vanaanen and J. Eisinger, *J. Membr. Biol.*, 1993, **135**, 83.
36 J. Teissie, J. F. Tocanne and A. Baudras, *Eur. J. Biochem.*, 1978, **83**, 77.
37 T. H. Huang, A. J. Desiervo and Q. X. Yang, *Biophys. J.*, 1991, **59**, 691.
38 P. F. Almeida, W. L. Vaz and T. E. Thompson, *Biochemistry*, 1992, **31**, 7198.
39 N. Kahya, D. Scherfeld, K. Bacia and P. Schwille, *J. Struct. Biol.*, 2004, **147**, 77.
40 O. Albrecht, H. Gruler and E. Sackmann, *J. Phys. (Paris)*, 1978, **39**, 301.
41 H. J. Galla, W. Hartmann, U. Theilen and E. Sackmann, *J. Membr. Biol.*, 1979, **48**, 215.
42 J. C. Crocker and D. G. Grier, *J. Colloid Interface Sci.*, 1996, **179**, 298.
43 M. Forstner, D. Martin and J. Käs, *Langmuir*, 2001, **17**, 567.
44 (*a*) P. R. Cullis, *FEBS Lett.*, 1976, **70**, 223; (*b*) A. Blume, in *Phospholipids Handbook*, ed. G. Cevc, Marcel Dekker, New York, 1993.
45 M. B. Forstner, D. S. Martin, A. M. Navar and J. A. Käs, *Langmuir*, 2003, **19**, 4876.
46 A. Miller, C. A. Helm and H. Möhwald, *J. Phys. (Paris)*, 1987, **48**, 693.
47 M. Lösche, E. Sackmann and H. Möhwald, *Ber. Bunsen-Ges. Phys. Chem.*, 1983, **87**, 848.
48 E. Weeks, Emory University, web site on SPT, co-author of downloadable IDL routines.
49 M. K. Cheezum, W. F. Walker and W. H. Guilford, *Biophys. J.*, 2001, **81**, 2378.
50 D. L. Ermak, *J. Chem. Phys.*, 1975, **62**, 4189.
51 J. Rädler and E. Sackmann, *Langmuir*, 1992, **8**, 848.
52 D. S. Martin, M. B. Forstner, A. M. Navar, J. A. Käs and C. Selle, 2004, in preparation.
53 P. Nassoy, W. R. Birch, D. Andelman and F. Rondelez, *Phys. Rev. Lett.*, 1996, **76**, 455.
54 H. M. McConnell, *Ann. Rev. Phys. Chem.*, 1991, **42**, 171.
55 P. Pieranski, *Phys. Rev. Lett.*, 1980, **45**, 569.
56 D. S. Martin, PhD thesis, University of Texas, Austin, TX, 2003.
57 V. Vogel and D. Möbius, *Thin Solid Films*, 1988, **159**, 73.
58 H. Haas and H. Möhwald, *Thin Solid Films*, 1989, **180**, 101.

